

## Article

# Experimental Investigation to Confirm the Presence of TiB<sub>2</sub> Reinforcements in the Matrix and Effect of Artificial Aging on Hardness and Tensile Properties of Stir-Cast LM4-TiB<sub>2</sub> Composite

Srinivas Doddapaneni <sup>1</sup>, Sathish Kumar <sup>2</sup>, Manjunath Shettar <sup>1</sup>, Suma Rao <sup>3</sup>, Sathyashankara Sharma <sup>1,\*</sup> and Gowrishankar MC <sup>1</sup>

- <sup>1</sup> Department of Mechanical and Industrial Engineering, Manipal Institute of Technology, Manipal Academy of Higher Education, Manipal 576104, India  
<sup>2</sup> Department of Mechanical Engineering, B.M.S. Institute of Technology and Management, Bangalore 560064, India  
<sup>3</sup> Department of Chemistry, Manipal Institute of Technology, Manipal Academy of Higher Education, Manipal 576104, India  
\* Correspondence: ss.sharma@manipal.edu



**Citation:** Doddapaneni, S.; Kumar, S.; Shettar, M.; Rao, S.; Sharma, S.; MC, G. Experimental Investigation to Confirm the Presence of TiB<sub>2</sub> Reinforcements in the Matrix and Effect of Artificial Aging on Hardness and Tensile Properties of Stir-Cast LM4-TiB<sub>2</sub> Composite. *Crystals* **2022**, *12*, 1114. <https://doi.org/10.3390/crust12081114>

Academic Editors: Weiwei Zhou and Huakang Bian

Received: 15 July 2022

Accepted: 7 August 2022

Published: 9 August 2022

**Publisher's Note:** MDPI stays neutral with regard to jurisdictional claims in published maps and institutional affiliations.



**Copyright:** © 2022 by the authors. Licensee MDPI, Basel, Switzerland. This article is an open access article distributed under the terms and conditions of the Creative Commons Attribution (CC BY) license (<https://creativecommons.org/licenses/by/4.0/>).

**Abstract:** The present work focuses on the effect of multistage solution heat treatment (MSHT) and artificial aging on two-stage stir-cast LM4 + TiB<sub>2</sub> (1, 2, and 3 wt.%) composites on the mechanical properties as compared to as-cast and single-stage solution heat-treated (SSHT) composites. Two novel tests, viz. the confirmation hardness test and the chemical analysis test, were performed to ensure the soundness of the casting and uniform distribution of TiB<sub>2</sub> within the matrix. Samples subjected to MSHT + aging at 100–200 °C displayed the highest hardness and UTS values compared to as-cast and SSHT + aging at 100–200 °C samples. Compared to as-cast alloy, peak-aged samples of 1–3 wt.% (MSHT + aging at 100 °C), hardness values improved from 107–150%, and UTS values improved from 47–68%. The presence of metastable phases ( $\theta'$ -Al<sub>2</sub>Cu and  $\theta''$ -Al<sub>3</sub>Cu) and of hard TiB<sub>2</sub> particles are the reason for the improvement in the properties. Peak aged LM4 + 3 wt.% TiB<sub>2</sub> composite displayed the highest hardness of 175 VHN and UTS of 251 MPa. Fracture analysis of the LM4 alloy showed dimple rupture, and its composites revealed quasi-cleavage fracture. Based on the overall results, the inclusion of TiB<sub>2</sub>, MSHT, and artificial aging treatment on the LM4 alloy significantly influenced the composites' mechanical properties.

**Keywords:** multistage solution heat treatment (MSHT); aging treatment; hardness; ultimate tensile strength (UTS); single-stage solution heat treatment (SSHT)

## 1. Introduction

Modern engine components must tolerate higher temperatures and strains than in the past due to increasingly rigorous pollution standards, resulting in a shrinking of engine size and reductions in fuel usage and emissions, necessitating the use of lighter automobiles [1]. Al-Si alloys are preferred in the automotive sector because they can overcome the above-mentioned challenges. Collecting information regarding Al-Si alloys and their composites is necessary, as well as establishing a relationship between microstructures and mechanical characteristics [2]. Among Al-Si alloys, LM4 (hypoeutectic alloy) has gained prominence in recent years due to its superior characteristics over A356 and other Al-Si alloys [3,4]. Si, Cu, and Mg are noted to be the most important alloying elements in hypoeutectic Al-Si alloys as they can provide sound strengthening effects [5]. T6 heat treatment is proven to be the most effective heat treatment approach for improving the mechanical properties (mainly strength) of LM4 alloy [6,7]. There will be a refinement in grains of eutectic silicon crystals as the solutionizing temperature increases, which increases the hardness and tensile strength values [8]. During aging, Al<sub>3</sub>Cu and Al<sub>2</sub>Cu precipitates are the main cause of the

strengthening of the A319 alloy [9]. The impact of precipitation hardening heat treatment on the hardness of LM4 alloy is clearly explained in our recent work, wherein LM4 samples subjected to MSHT + aging at 100 °C displayed the highest hardness values when compared to as-cast, SSHT + aging at 100 and 200 °C, and MSHT + aging at 200 °C samples [10]. The tensile strength of Al-Si alloys mainly depends on the porosity level and heat treatment. The  $\beta$ -Al<sub>5</sub>FeSi intermetallic is expected to significantly reduce the ductility and fracture strength of the alloy, which relies on the morphology of crystals present in the matrix influencing the reduction;  $\alpha$ -iron Chinese script is more resistant to stress than  $\beta$  intermetallic [11]. Cracks typically propagate through the Al<sub>2</sub>Cu fracture along with shattered Si particles rather than through matrix decohesion [12]. Li et al. [2] studied the damage mechanics of the A319 alloy under tensile loading. The results concluded that crack initiation and propagation always occur through the hard inclusions (Si, Al<sub>2</sub>Cu, and Fe intermetallics) in the stress-affected regions [13]. Samuel et al. [14] stated that coarse acicular and needle-shaped Si particles are the main reason for crack initiation. Han et al. [15] stated that in A319 alloys, the tensile properties mainly depend on eutectic silicon, SHT (to obtain a full dissolution of strengthening elements), and the combined effects of dissolution of the Al<sub>2</sub>Cu phase and Si particle characteristics. Rincon et al. [16] studied the tensile behavior of the A319 alloy in both heat-treated (T7) and as-cast conditions at different working temperatures. The results concluded that there was a 156% improvement in the alloy's tensile strength after heat treatment. Furthermore, above 200 °C, the work hardening properties attained by the heat treatment started to drop. Samuel et al. [11] studied the fracture behavior of A319 under T5 and T6 conditions. Based on the findings, they concluded that regardless of dendritic arm spacing, crack initiation always happens through the fragmentation of Si and  $\beta$  platelets and propagation via  $\beta$  platelets. Zhu et al. [17] investigated the tensile behavior of Al-Si alloys under T6 conditions. They stated that T6-treated alloy displayed better UTS, YS, and EL when compared to a non-heat-treated alloy. This improvement is due to precipitation hardening of Mg<sub>2</sub>Si and spheroidization of eutectic Si. TiB<sub>2</sub>-reinforced aluminum matrix composites outperform other reinforced AMCs in terms of tribological and mechanical properties [18]. Karbalaei et al. [19] fabricated Al-Si composites with TiB<sub>2</sub> (nano- and micro-sized) particles and analyzed the effect of TiB<sub>2</sub> on the tensile behavior of the composites. They concluded that the addition of TiB<sub>2</sub> improved the tensile values to 1.5 vol% and a further increase in addition to TiB<sub>2</sub> caused agglomeration mainly in the case of nano-sized TiB<sub>2</sub>; also, the main reason for the fracture in the prepared composite was found to be silicon cracking and debonding of TiB<sub>2</sub> with the Al matrix. TiB<sub>2</sub> reinforcement powders with high tensile strength, a high melting point, and greater chemical stability at high temperatures are just a few of the benefits of using it as an aluminum matrix reinforcement material [20]. Vandersluis et al. [21] performed SHT at 500 °C/0.5–48 h on the A319 alloy, and from the results, they concluded that when heated above 500 °C, dissolution of Al<sub>2</sub>Cu and modification of eutectic Si were observed, which enhanced the mechanical properties of A319. Akhil et al. [22] performed precipitation hardening treatment (SHT–500 °C, aging–170°/1–16 h) on the Al–5Si–3Cu alloy, and from the results, they concluded that, after precipitation hardening treatment, eutectic Si underwent necking and the average particle size reduced, while the highest hardness of 110 BHN was achieved when aged at 170 °C/7 h. Han et al. [15] performed single-step, two-step, and triple-step SHT (the SHT temperature used was 450, 490, 500, and 520 °C) followed by aging at 155 °C/5 h on the A319 alloy. From the results, it was concluded that, when subjected to single-step SHT and aging, Cu dissolution and modification of eutectic Si were not observed; similarly, for triple-step SHT and aging, incipient melting of Cu occurred, which caused a drop in the mechanical properties of A319. When subjected to two-step SHT and aging, dissolution of Al<sub>2</sub>Cu and spheroidization of Si were observed, which caused improvement of the mechanical properties of A319. Sokolowski et al. [23] also confirmed that A319 samples when subjected to multistage SHT followed by aging displayed better mechanical properties when compared to single-stage SHT and aging. Mohamed et al. [24] suggested that when performing multistage SHT, the SHT temperature

should not exceed 520 °C, because when subjected to 530 °C, a drop in the mechanical properties were observed. Based on a thorough review of the literature, it was noted that there has been little research on multistage solution heat treatment (MSHT) to enhance the mechanical properties (hardness, tensile strength) of TiB<sub>2</sub>-reinforced composites as compared to as-cast and single-stage solution heat-treated (SSHT) composites. Investigating changes in solution treatment for eutectic phase grain refinement and controlled precipitation of aluminum-rich intermetallics to strengthen the matrix is worthwhile. The influence of MSHT on LM4 + TiB<sub>2</sub> composites was investigated in comparison to SSHT with age hardening treatment. As a part of this novel work, the present study mainly deals with two new experimental methods, i.e., to confirm the percentage of reinforcement presence in the matrix during the stir-casting process and to prove the uniform distribution of reinforcement in the matrix other than optical micrograph or SEM analysis.

## 2. Materials and Methods Used in this Study

### 2.1. Methodology

The detailed methodology used in the present study is explained in this section. LM4 + TiB<sub>2</sub> composites were prepared using a two-stage stir-casting method, and age hardening treatment was carried out to check the peak hardness of cast composite samples and compare the hardness between heat-treated and as-cast samples of both the alloy and its composites.

Confirmation tests were conducted on as-cast composite samples to validate the uniform distribution of TiB<sub>2</sub> in the LM4 matrix. Microstructural analysis was performed through the Scanning Electron Microscope (SEM)-EVO MA18. The methodology followed in the present work is displayed in Figure 1.

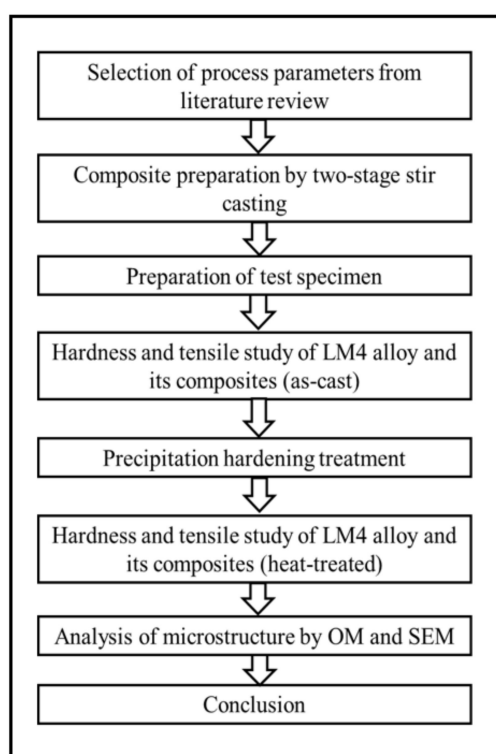


**Figure 1.** Flow chart of the methodology followed in the present study.

### 2.2. Matrix and Reinforcement Material

Table 1 shows the chemical composition of the LM4 alloy obtained from BUREAU VERITAS (INDIA) PRIVATE LIMITED, Bangalore, and the test method used was ASTM E-1251-2011. Table 2 shows the properties of the LM4 alloy and TiB<sub>2</sub> reinforcement, respectively. TiB<sub>2</sub> powder having an average particle size of 6.765 μm was acquired. The

SEM image and EDAX report of the  $\text{TiB}_2$  powder are shown in Figure 2 to confirm the presence of Ti and B.

**Table 1.** Composition (wt.%) of LM4 alloy.

Material	Si	Cu	Mg	Sn	Ni	Fe	Ti	Mn	Al
wt.% (Actual)	5.925	2.476	0.176	0.045	0.03	0.641	0.045	0.121	Bal.
wt.% (Standard)	4–6	2–4	0–0.20	0–0.1	0–0.3	0–0.8	0–0.2	0.2–0.6	Bal.

**Table 2.** Properties of LM4 alloy and  $\text{TiB}_2$  reinforcement [4,19].

Properties	LM4	$\text{TiB}_2$
Density ( $\text{g}/\text{cm}^3$ )	2.75	4.52
Hardness (VHN)	68–83	960
Melting point ( $^\circ\text{C}$ )	660	2790

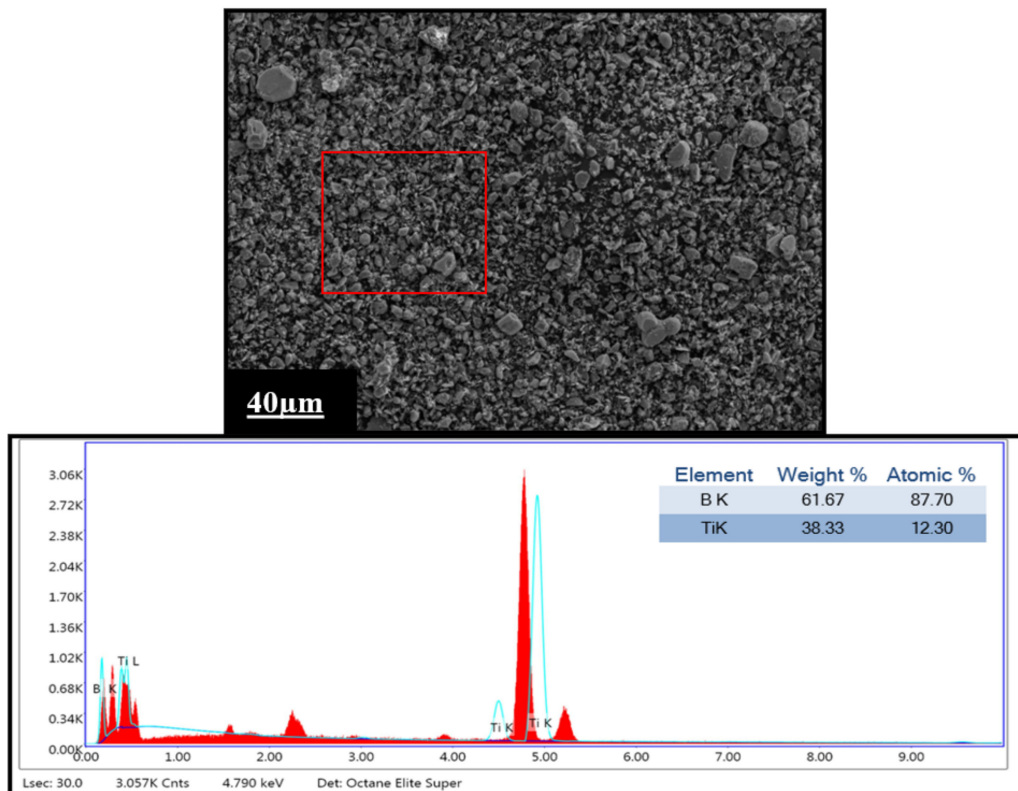


**Figure 2.** SEM and EDAX of  $\text{TiB}_2$  reinforcement powder.

### 2.3. Composite Preparation

The preparation of the LM4 +  $\text{TiB}_2$  composites (1, 2, and 3 wt.%) is given in the flow chart (Figure 3), along with the stir-casting process and cast composites' bar and pencil mold samples in Figure 4. After successfully preparing the composites, cast samples were analyzed using SEM to validate the uniform distribution of  $\text{TiB}_2$  in the LM4 matrix. Two new confirmation test methods (confirmation hardness test and chemical analysis test) were also carried out to check the soundness of casting and the uniform distribution of the reinforcement.

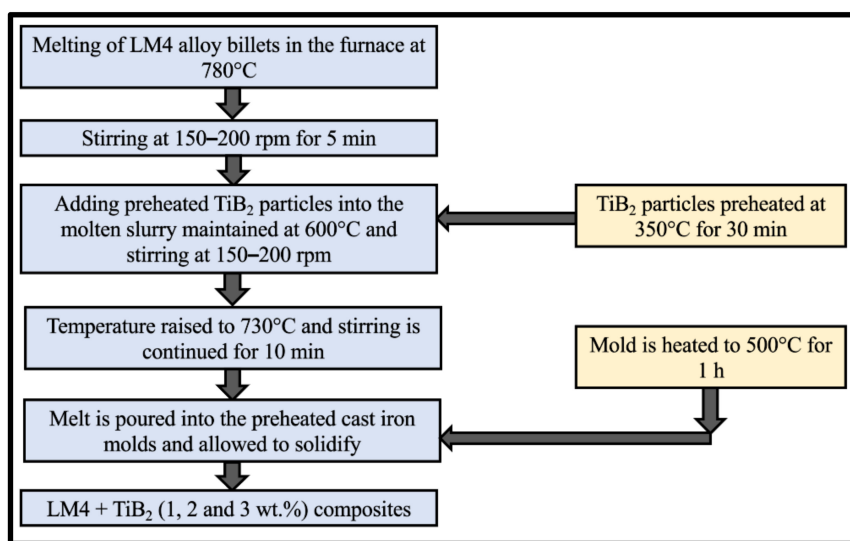


**Figure 3.** Flow chart for the fabrication of LM4 + TiB<sub>2</sub> composites.



**Figure 4.** Experimental setup of stir-casting method used in the present work.

#### 2.4. Hardness and Tensile Test

Hardness tests were performed using a Micro Vickers Hardness Tester, Model-MMT X 7A, a load of 200 gmf, and a 15 s dwell time. Before hardness testing, all samples were polished (mirror finish) using automated disc polishing equipment to eliminate impurities and oxides produced during heat treatment.

Figure 5 shows a tensile specimen produced in accordance with the ASTM-E8M standard. Tensile tests were performed using an Electronic Tensometer, Model-PC-2000/605/06. The load cell value was maintained at 20 kN with break test mode, and the speed was maintained at 1 mm/min. The tensile test was carried out for both peak-aged and as-cast samples of LM4 alloy and its composites.

#### 2.5. Age Hardening/Precipitation Hardening Treatment

MSHT, SSHT, and aging at 100 and 200 °C were conducted on as-cast samples. The detailed procedure of the heat treatment is shown in the schematic diagram (Figure 6). As per the literature [23], eutectic Si modification and copper phase dissolution were not observed when SSHT was performed on the A319 alloy, but when subjected to MSHT, it showed better behavior (improved properties). Hardness, tensile test, and fracture analysis

were performed on heat-treated and as-cast samples. XRD analysis was carried out on the age-hardened samples using Rigaku-Miniflex600.



**Figure 5.** Tensile sample before and after machining as per the standards.

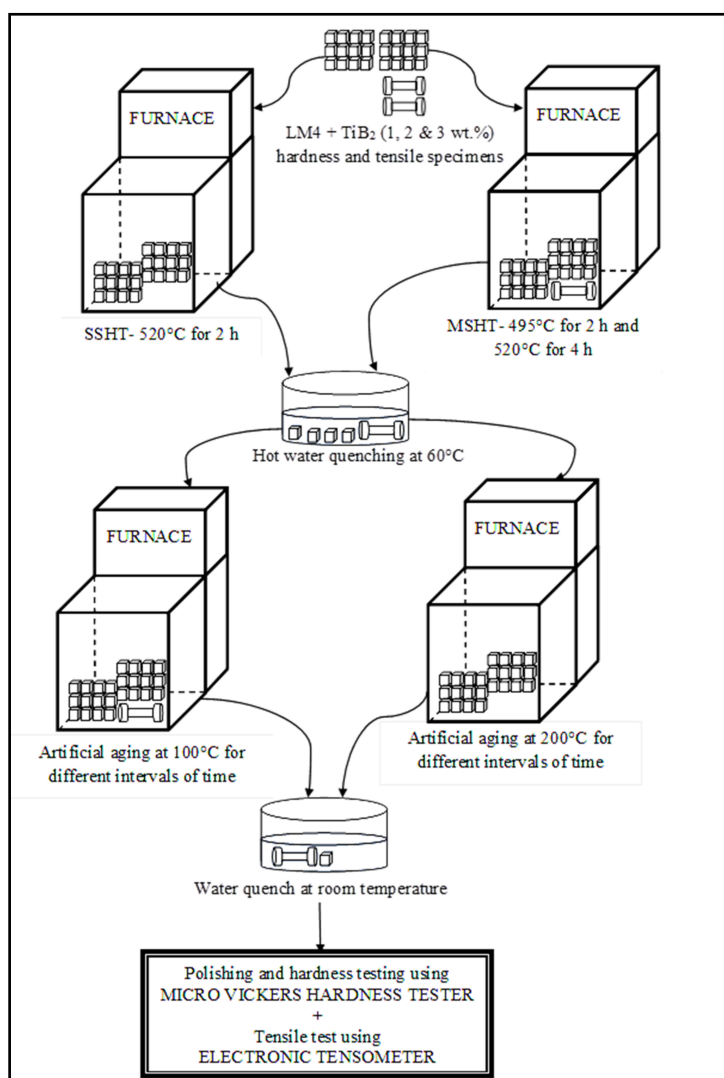


**Figure 6.** Process chart of precipitation hardening treatment.

### 3. Results and Discussion

#### 3.1. Microstructure Studies

To achieve better mechanical properties from the cast composites, the distribution of reinforcements in the matrix material should be uniform, and reinforcement agglomeration should be avoided. As per the literature [25], it was confirmed from optical microscope (OM) images that reinforcement was distributed uniformly in the matrix material and that particle agglomeration was not seen (1–3 wt.%), whereas in LM4 + TiB<sub>2</sub> (5 wt.%), composite agglomeration was observed [26]. Hence, it is not explored here for further analysis. Figure 7 depicts the SEM and EDAX analysis of LM4 + 3 wt.% TiB<sub>2</sub> supporting the reinforcing powder's presence and homogeneous distribution in the matrix alloy.

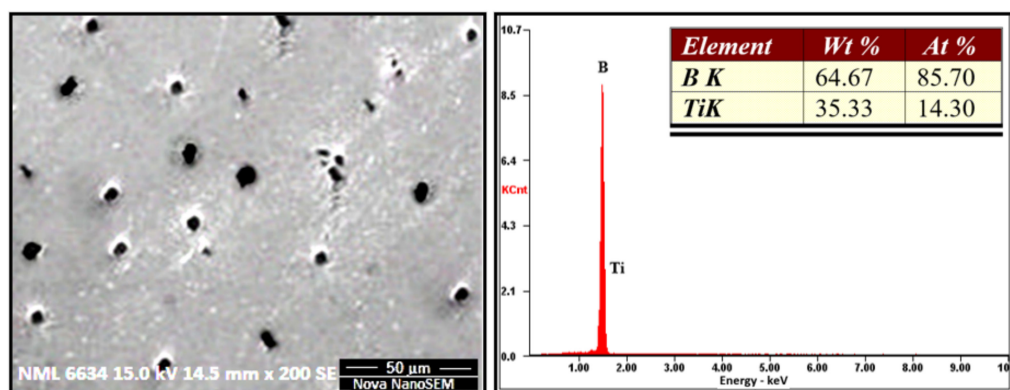


**Figure 7.** SEM and EDAX of LM4 + 3 wt.% TiB<sub>2</sub> composite sample.

#### 3.2. Confirmation Test through Chemical Analysis and Hardness Measurement

To confirm the homogenous distribution of TiB<sub>2</sub> throughout the composite, five identical specimens were cut from each composite bar at a distance of 15, 30, 45, 60, and 75 mm from the lower end, as shown in Figure 8, and they were subjected to a hardness test with five trials for each specimen. The hardness results confirmed that the hardness distribution was uniform throughout the sample, which indicated the uniform distribution of the reinforcement within the matrix. Figure 9 shows the hardness distribution graph of the composite samples.

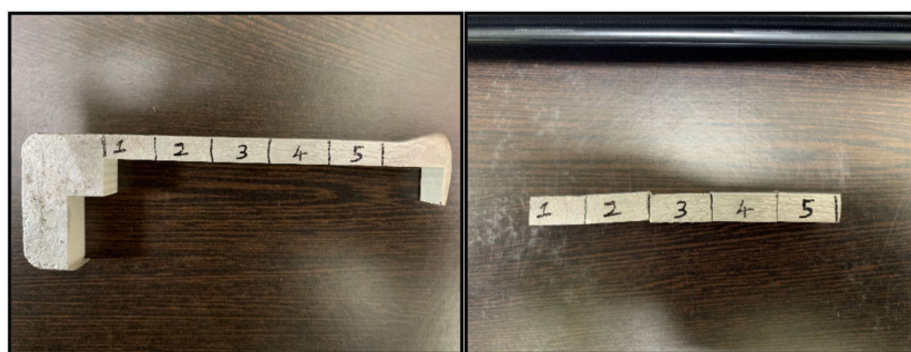


**Figure 8.** Samples for confirmation test.

The LM4 alloy and LM4 + 3 wt.% TiB<sub>2</sub> composite samples were subjected to a chemical confirmation test by dissolving these samples in concentrated sodium hydroxide (NaOH) to confirm the amount of reinforcement present in the 3 wt.% composites. Before testing, samples were heated at 100 °C to remove moisture, and initial weights were recorded. Samples were kept in separate beakers and were heated on a hotplate at 50 °C with 20% concentrated NaOH (about 125 mL) in them; this was heated until the acid boiled. The aluminum alloy dissolved in the acid completely during heating followed by 10 h of soaking. During boiling, the TiB<sub>2</sub> reinforcement particles and other residues float on top

of the acid's surface. The residue formed after the complete evaporation of the aluminum was poured into ashless Whatman filter paper, and it was folded and placed in an oven at 100 °C for 2 h to remove the moisture. The initial weights of two crucibles were noted, and then, the filter paper was burnt in those crucibles by heating using a Bunsen burner at a high temperature (700 °C), then the residue powder was collected.

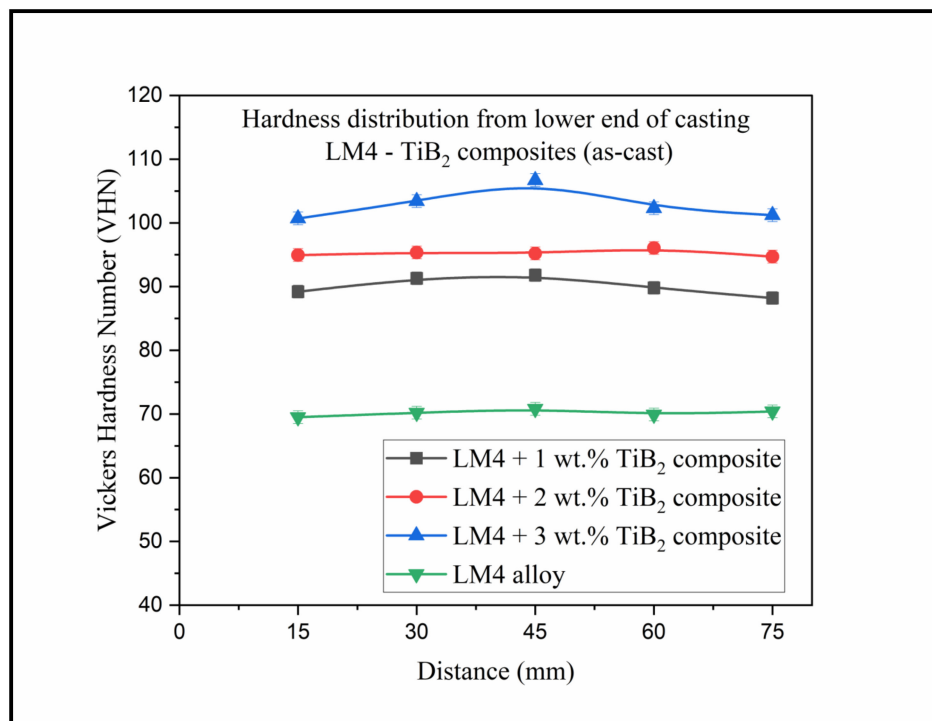


**Figure 9.** Hardness distribution graph from the lower end of the cast LM4 alloy and its composites.

For 1600 g of LM4 alloy, 48 g (3 wt.%) of TiB<sub>2</sub> was added during stir-casting. The initial weight of the samples used in this study was 2 g each. The theoretical weight of the reinforcement in the 2 g composite sample by calculation was 0.06 g. Experimental results of the weights are shown in Table 3.

**Table 3.** Experimental data of the chemical analysis test.

Type	Value
Initial weight of alloy (LM4) and composite (LM4 + 3 wt.% TiB <sub>2</sub> )	2 g each
Initial weight of two crucibles	15.8969 g (alloy) and 15.9494 g (composite)
Final weight of two crucibles after burning filter paper	15.9031 g (alloy) and 16.01342 g (composite)
Alloy residue weight	15.9031 – 15.8969 = 0.0062 g (alloy residue weight is negligible)
Composite residue weight	16.01342 – 15.9494 = 0.06402 g
Weight of reinforcement in composite	0.06402 – 0.0062 = 0.05782 g
wt.% for reinforcement in composite	((0.06402 – 0.0062)/2) × 100 = 2.891%

Therefore, based on the calculations, the quantity of foreign particles present in the alloy were extremely low (viz., 0.31%), indicating that the alloy was pure with almost no impurities and that almost 96% of the reinforcements were present in the matrix of the cast composite. The process of this chemical analysis test and the EDAX report of the powder collected are

shown in Figure 10. The existence of the Ti and B elements was verified in the EDAX report of the powder collected, confirming the efficiency of the chemical analysis test.

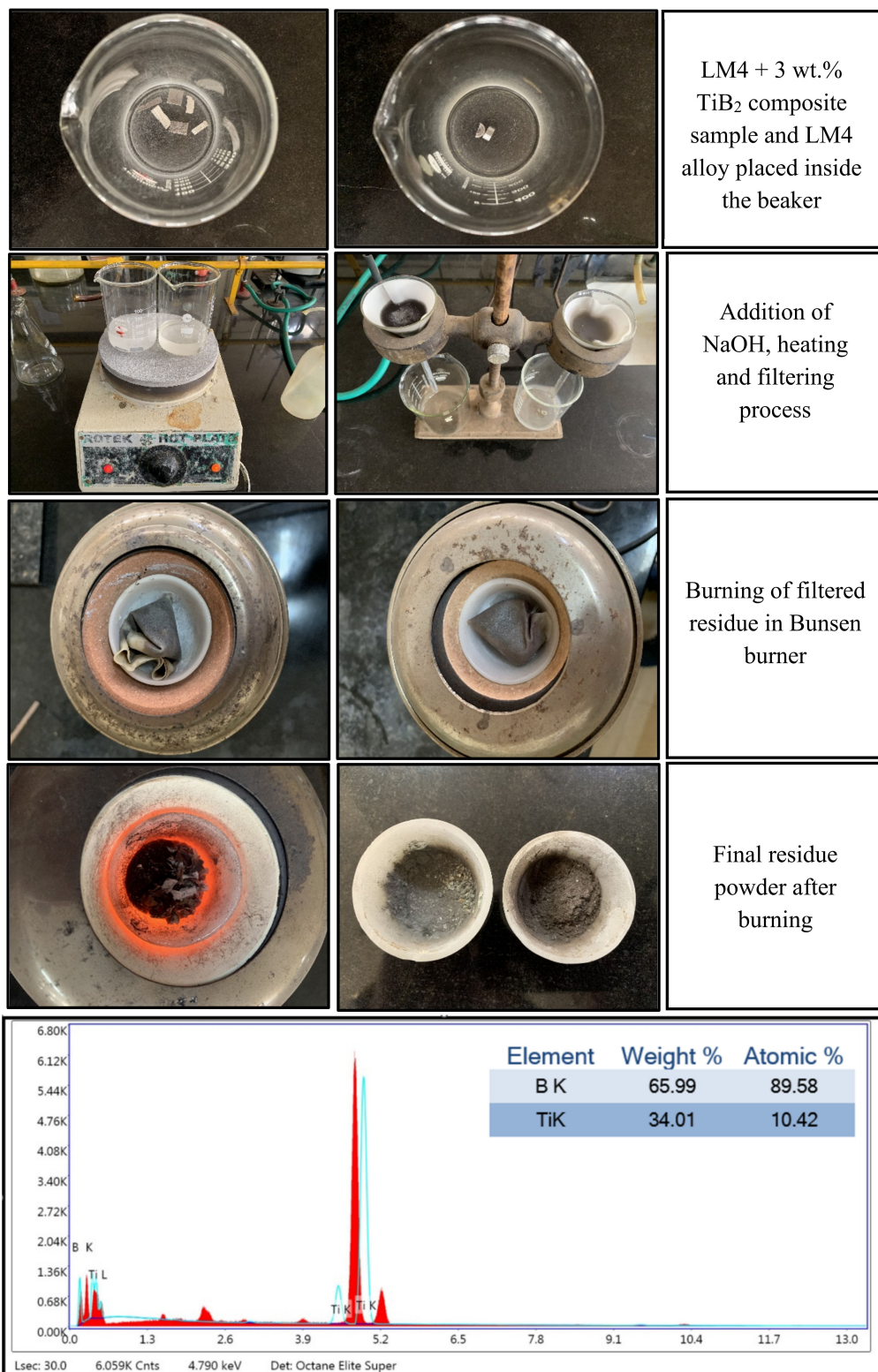


**Figure 10.** Process of chemical analysis test and EDAX report to confirm the presence of  $\text{TiB}_2$  in the LM4 matrix.

### 3.3. Aging Curve and Hardness

A hardness test was performed on the LM4 alloy and its composites for heat-treated and as-cast conditions. Heat-treated samples displayed better hardness values than as-cast samples. The hardness of the LM4 alloy and its composites improved gradually with aging. After attaining peak aging, the hardness values gradually decreased. When aged at 100 and 200 °C, as the wt.% of reinforcements increased, the time to reach peak hardness reduced. The summary of the hardness improvement is as follows: the as-cast alloy and its composites (1, 2, and 3 wt.%) displayed a hardness of 70, 89, 95, and 103 VHN, respectively. When compared to the LM4 alloy, samples after SSHT and MSHT showed an 80–150% and 65–120% increase in hardness when aged at 100 and 200 °C. The presence of hard TiB<sub>2</sub> particles is the main reason for the hardness improvement in the as-cast composites. The obtained results are in line with the published research observations [26–28]. Figures 11a–d and 12a–d display the hardness values of the SSHT and MSHT samples aged at 100 and 200 °C, respectively, with respect to the aging time. For every combination, aging at 100 °C resulted in greater hardness than aging at 200 °C. Still, the duration to reach peak hardness was less for samples aged at 200 °C, which can be related to aging kinetics [29]. The MSHT samples displayed higher hardness as they possessed more precipitates than the SSHT samples [10]. The peak-aged samples have higher hardness than the as-cast and other samples because of the formation of phases θ'-Al<sub>2</sub>Cu and θ"-Al<sub>3</sub>Cu (Figure 13) as they precipitate along and within grain boundaries [30,31]; also, a minor portion of the Mg<sub>2</sub>Si phase contributed to the improvement of the hardness in the treated composites; as a result, the LM4 + TiB<sub>2</sub> (3 wt.%) MSHT samples aged at 100 °C attained the maximum hardness. A comparison of the peak hardness of the LM4 alloy and its composites is shown using a bar graph in Figure 14. On average, when compared to as-cast samples of the alloy and composites, the SSHT + aged at 200 °C samples showed a 15% improvement in hardness, the SSHT + aged at 100 °C showed a 25% improvement, the MSHT + aged at 200 °C showed a 52% improvement, and the MSHT + aged at 100 °C showed a 72.25% improvement in hardness. Compared to the LM4 (MSHT + aged at 100 °C) peak hardness, LM4 + TiB<sub>2</sub> (1, 2, and 3 wt.%) (MSHT + aged at 100 °C) achieved a 9, 20, and 30% improvement. At every stage, MSHT, lower aging temperature, and larger wt.% of reinforcement in the matrix were favorable for excellent peak hardness value (Figure 14).

### 3.4. Tensile Properties

Tensile tests were conducted on as-cast, and peak-aged samples of the LM4 alloy and LM4 + TiB<sub>2</sub> composites, and the tensile curves of the as-cast LM4 and peak-aged LM4 + 3 wt.% TiB<sub>2</sub> composite are shown in Figure 15a,b, while the average values of the UTS readings of the as-cast and peak-aged samples are shown in Figure 15c. From Figure 15a,b, we can see that, for the as-cast LM4 sample, the peak load and peak displacement were found to be 4838 N and 1.26 mm, whereas for the peak-aged LM4 + 3 wt.% TiB<sub>2</sub> composite sample, the peak load and peak displacement were found to be 8120 N and 2.19 mm. This increase in the peak load of the LM4 + 3 wt.% TiB<sub>2</sub> composite sample and the strengthening behavior of the LM4 composites were due to the load-bearing capability of the reinforcement particles. The presence of hard reinforcement particles caused the improvement in the load bearing capacity of the composites. Reinforcements and dislocations caused improvement in the resistance to crack propagation [19]. The increase in the tensile strength of the composites was mainly because of intermetallic precipitates, which restricted the dislocation motion and reduced plastic deformation. Higher dislocation density resulted from higher particle concentration and lower aging temperature. Because of the applied load, the matrix had a restricted plastic flow; these hard intermetallics caused a dislocation pileup. The interaction of dislocations with reinforcement, intermetallic, and grain boundaries synergized the alloy strengthening [32]. From Figure 15c, it is observed that the composites displayed higher UTS values than the alloy in the as-cast, as well as in the peak-aged conditions. Compared to the as-cast UTS value of LM4, its composites with 1, 2, and 3 wt.% of TiB<sub>2</sub> in the as-cast condition displayed a 25, 33, and 45% improvement; similarly, in the peak-aged (MSHT + aging at 100 °C) condition, a 47, 57, and 68% improvement in UTS was observed. Similar to the hardness results, the samples

subjected to MSHT + aging at 100 °C demonstrated greater UTS values, with the composite containing 3 wt.% TiB<sub>2</sub> having the highest.

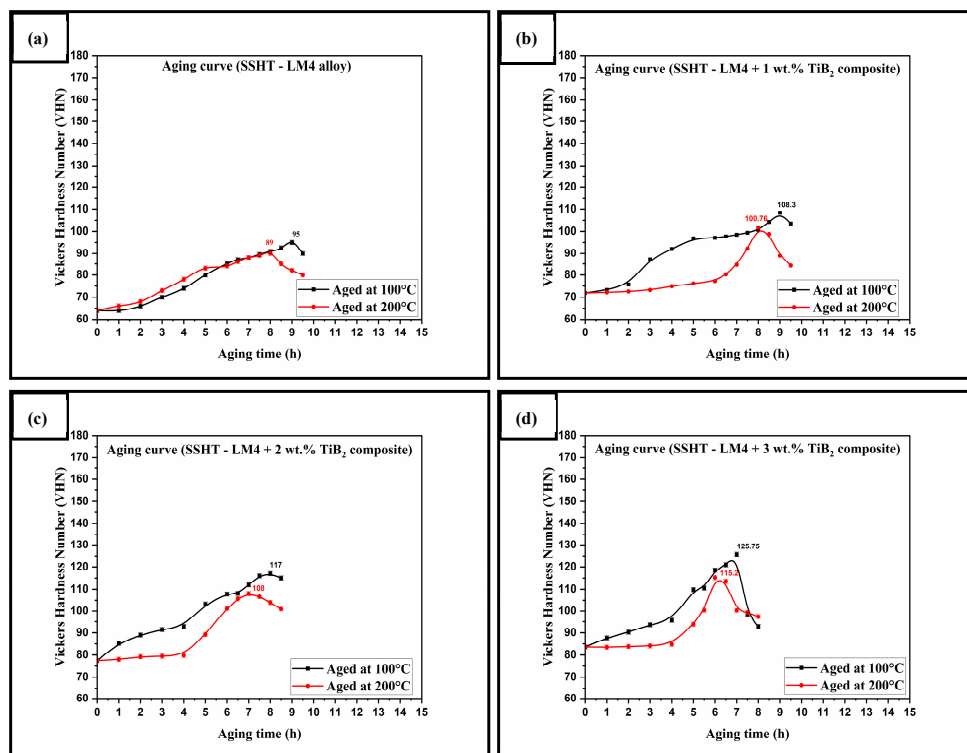


**Figure 11.** (a–d) Aging curves of the precipitation-hardened (SSHT + artificial aging) LM4 alloy and its composites.

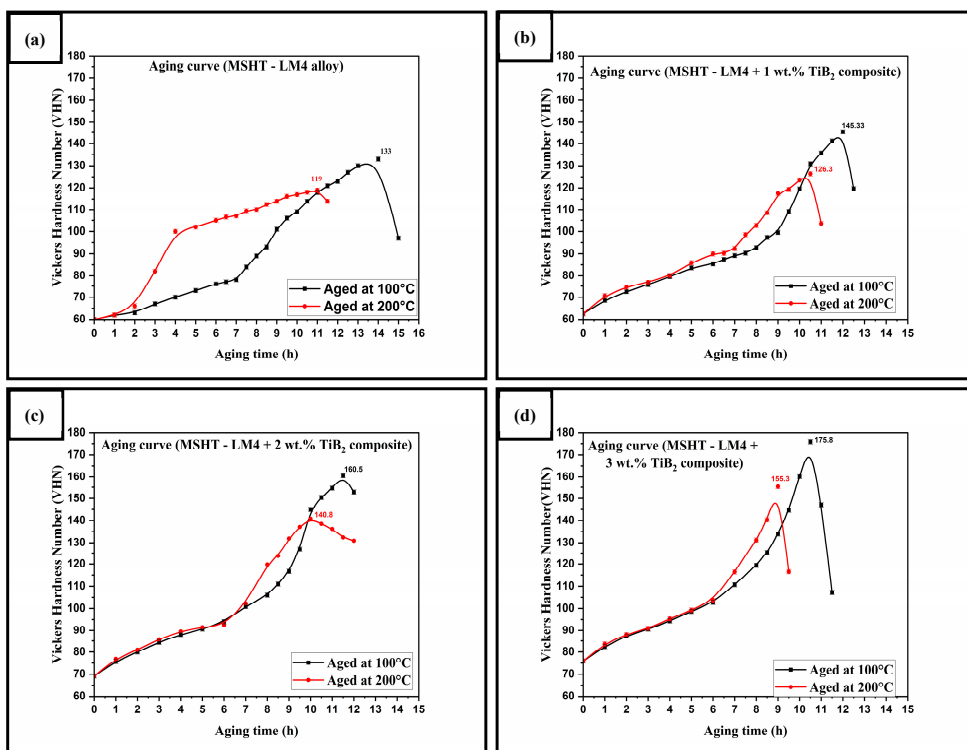


**Figure 12.** (a–d) Aging curves of the precipitation-hardened (MSHT + artificial aging) LM4 alloy and its composites.

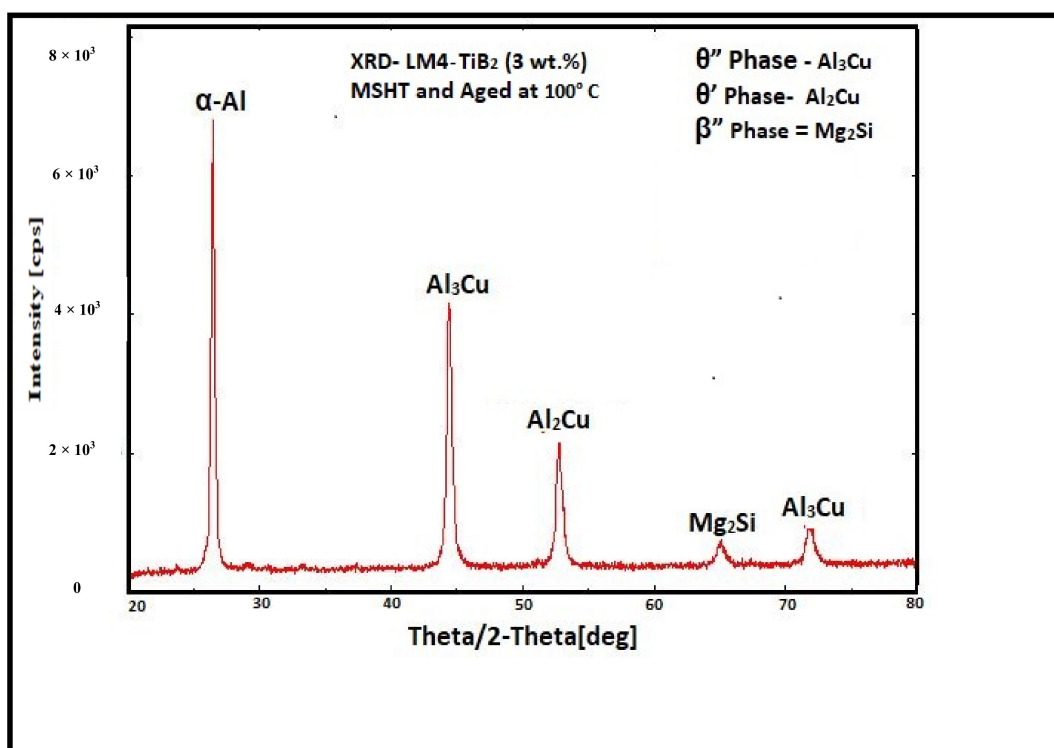


**Figure 13.** XRD of the LM4 + 3 wt.% TiB<sub>2</sub> composite sample (MSHT and aged at 100 °C) to confirm the presence of different types of precipitates.

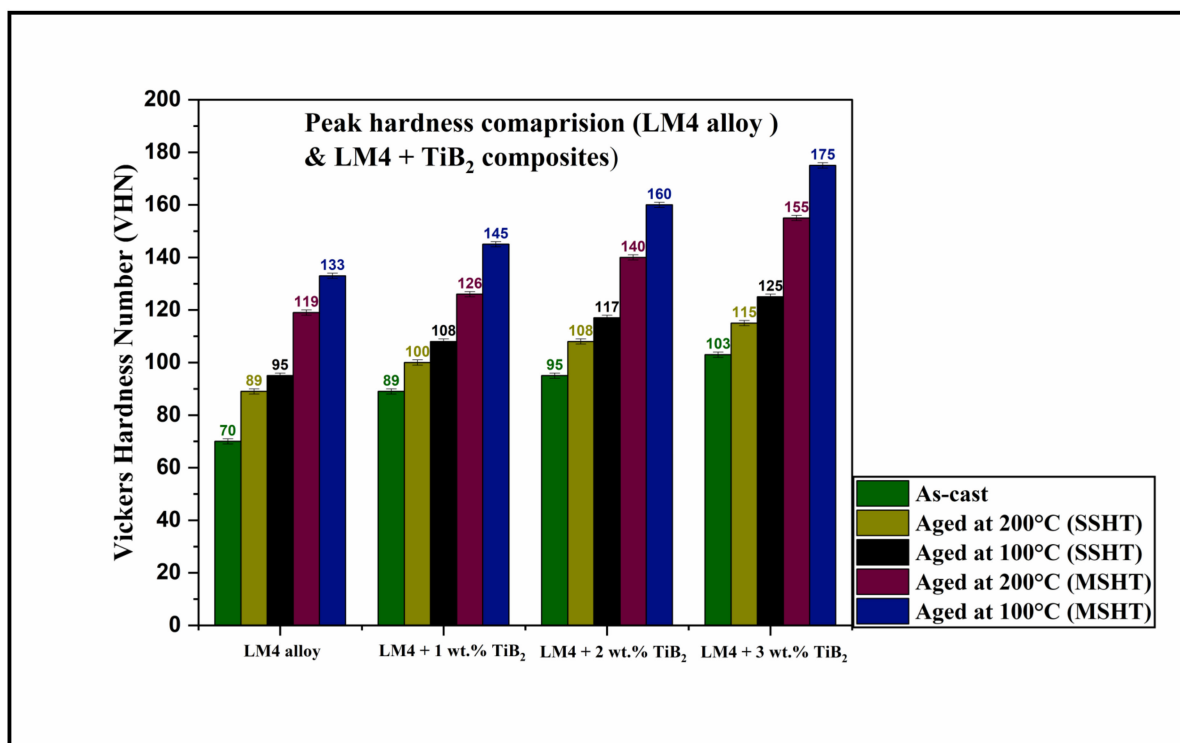


**Figure 14.** Comparison of the peak hardness of the LM4 alloy and its composites under different solutionizing and aging conditions.

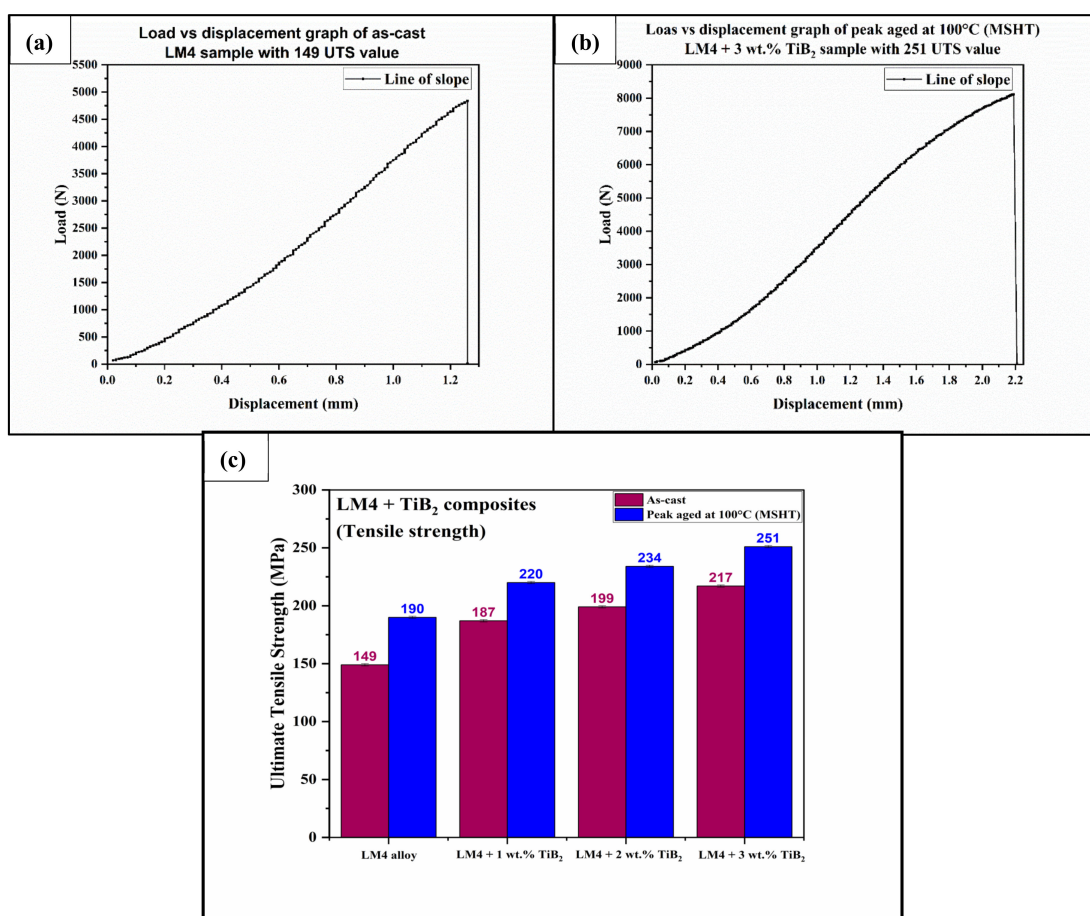


**Figure 15.** (a,b) Tensile curves of the as-cast LM4 and peak-aged LM4 + 3 wt.% TiB<sub>2</sub> composite. (c) Comparison of UTS values of the as-cast and peak-aged samples.

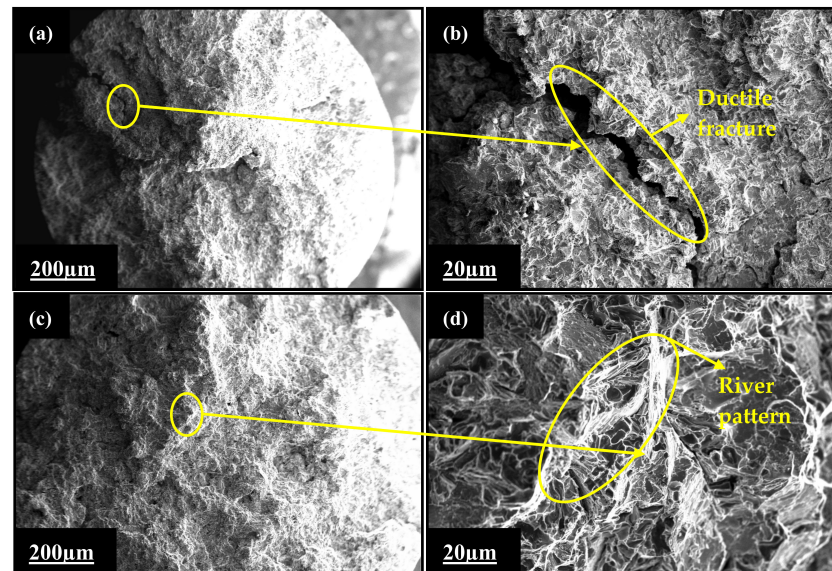
### 3.5. Fracture Surface Analysis of the LM4 Alloy

SEM was used to evaluate the fracture surface of the tensile test sample. Figure 16 depicts the fractographs of the LM4 alloy (as-cast and peak-aged at 100 °C). Many fine equiaxial dimples were visible on the fracture surface, and the fracture mechanism was largely dimple rupture (Figure 16a,b). Numerous cuplike depressions were seen, which are referred to as primarily dimple rupture in Figure 16b at greater magnification. Some micro-voids were seen near the grain boundaries. The existence of a river pattern indicated that the mode of fracture was entirely ductile. As a result, the as-cast LM4 alloy had lower UTS values. The fracture surface of a peak-aged specimen (100 °C) is shown in Figure 16c,d. In peak-aged conditions, the density of the dimples was higher, more equally distributed, and smaller, suggesting the production of a greater quantity of micro-voids. The dimples on the fracture surface of the artificially aged specimen were smaller than those on the as-cast LM4 alloy. The size of the dimple is directly related to the strength and ductility [33]. The finer the dimple size, the greater the strength and ductility, and vice versa. As a result, the artificially aged specimen had greater UTS values than the untreated LM4 alloy [17].

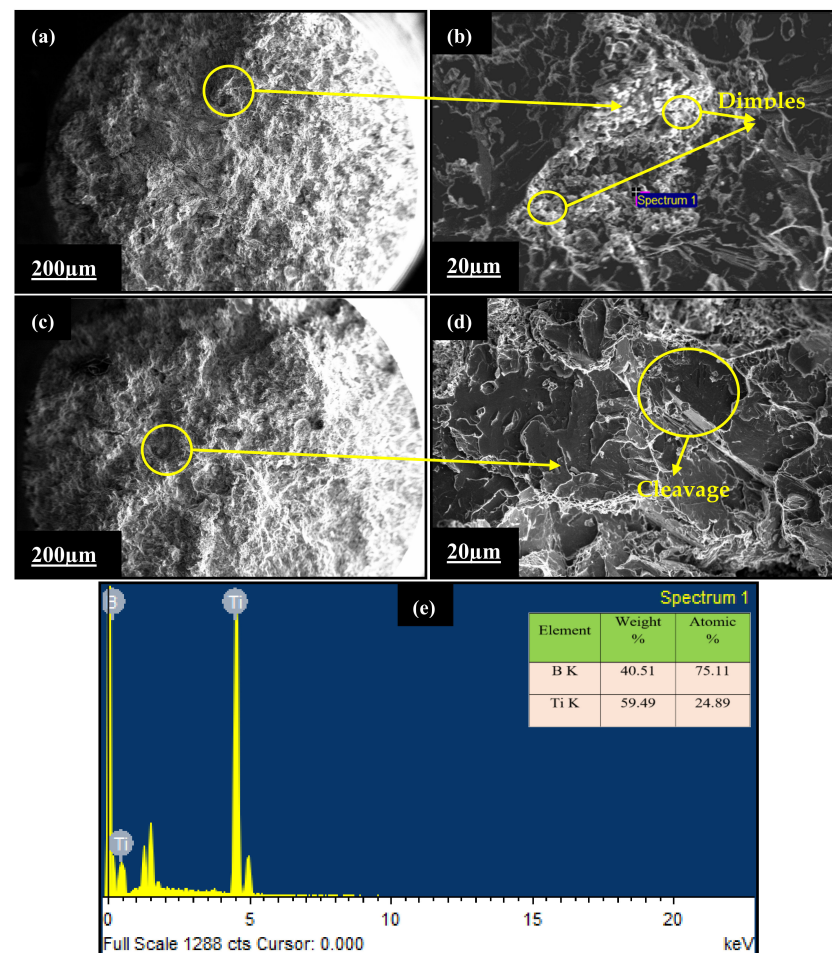
### 3.6. Fracture Surface Analysis of LM4 + TiB<sub>2</sub> Composites

Figure 17a,b depict an LM4 + 3 wt.% TiB<sub>2</sub> as-cast composite fracture surface. Compared to the LM4 alloy, there was a significant drop in dimple density. Fracture in a localized zone may be caused by shear, resulting in the creation of elongated dimples. The fracture mechanism observed in the peak-aged sample at 100 °C (Figure 17c,d) was a dimple rupture. Dimples form when multiple nucleation sites are activated, forming micro-voids and their subsequent coalescence. Nucleation sites can be inclusions, second phase particles, grain boundary dislocation pileups, and so on. The distribution of these particles/defects considerably impacts the fracture

type [34]. The creation of dimples of varied sizes is caused by the non-uniform distribution of such particles/defects of varying sizes. In a few instances, there is also evidence of quasi-cleavage fracture [35]. Quasi-cleavage is limited and shows cleavage and plastic deformation properties (Figure 17d). In Figure 17e, the EDAX confirms the presence of Ti and B.



**Figure 16.** Fracture analysis of the (a,b) as-cast and (c,d) peak-aged LM4 alloy tensile sample.



**Figure 17.** Fracture analysis of the (a,b) as-cast and (c,d) peak-aged LM4 + 3 wt.% TiB<sub>2</sub> tensile sample. (e) EDAX report of the same.

#### 4. Conclusions

This paper aimed to determine the effect of MSHT and artificial aging on the mechanical properties of the LM4 alloy and LM4+ TiB<sub>2</sub> composites. The following conclusions were drawn based on the results obtained:

- The two-stage stir-casting process was proven to be the most effective method for producing composites; the hardness test confirmed the soundness of the casting, and chemical analysis confirmed the quantity of reinforcement present in the cast samples.
- There were 27–47% and 25–45% improvements in the hardness and UTS values observed in the LM4 + TiB<sub>2</sub> (1, 2, and 3 wt.%) composites when compared to the as-cast LM4 alloy; this improvement in the properties was in large part due to the presence of hard TiB<sub>2</sub> particulates.
- The MSHT samples possessed a greater number of precipitates, and because of which, they displayed higher hardness values than the SSHT and as-cast samples. The MSHT samples aged at 100 °C displayed higher hardness and UTS values when compared to the SSHT samples aged at 100 and 200 °C. As shown in the XRD analysis, the Al<sub>2</sub>Cu and Al<sub>3</sub>Cu phases were the major reason for improving the properties such as the hardness and tensile strength.
- Compared to the as-cast alloy, the MSHT composite samples aged at 100 °C (peak-aged) showed a 107–150% and 47–68% improvement in hardness and tensile values, respectively.
- The LM4 alloy's fracture mechanism was mostly dimple rupture. The base alloy's peak-aged tensile fracture surface indicated a mixed mode of failure. The fracture surface of the TiB<sub>2</sub>-reinforced composite fracture revealed quasi-cleavage fracture and plastic deformation.

**Author Contributions:** Conceptualization, S.D., S.S. and G.M.; methodology, S.D., S.K., M.S., S.R. and G.M.; software, S.K. and G.M.; investigation, S.D., S.R. and G.M.; data curation, M.S., S.S. and G.M.; writing—original draft preparation, S.D. and G.M.; writing—review and editing, M.S. and S.S.; supervision, S.S. and G.M.; project administration, S.S. and G.M. All authors have read and agreed to the published version of the manuscript.

**Funding:** This research received no external funding.

**Institutional Review Board Statement:** Not applicable.

**Informed Consent Statement:** Not applicable.

**Data Availability Statement:** Not applicable.

**Acknowledgments:** The authors would like to acknowledge the Manipal Academy of Higher Education, Manipal, for providing the infrastructural facility to conduct the experimental works.

**Conflicts of Interest:** The authors declare no conflict of interest.

#### References

1. Ceschini, L.; Morri, A.; Toschi, S.; Seifeddine, S.; Messieri, S. The influence of cooling rate on microstructure, tensile and fatigue behavior of heat-treated Al-Si-Cu-Mg alloys. *Mater. Sci. Forum* **2017**, *884*, 81–92. [[CrossRef](#)]
2. Li, Z.; Limodin, N.; Tandjaoui, A.; Quaeghebeur, P.; Witz, J.F.; Balloy, D. Influence of Fe content on the damage mechanism in A319 aluminum alloy: Tensile tests and digital image correlation. *Eng. Fract. Mech.* **2017**, *183*, 94–108. [[CrossRef](#)]
3. Tash, M.; Samuel, F.H.; Mucciardi, F.; Doty, H.W. Effect of metallurgical parameters on the hardness and microstructural characterization of as-cast and heat-treated 356 and 319 aluminum alloys. *Mater. Sci. Eng. A* **2007**, *443*, 185–201. [[CrossRef](#)]
4. Poria, S.; Sahoo, P.; Sutradhar, G. Tribological characteristics of stir-cast Al-TiB<sub>2</sub> metal matrix composites in lubricated condition using taguchi based grey relation analysis. *Mater. Today Proc.* **2018**, *5*, 23629–23637. [[CrossRef](#)]
5. Abdelaziz, M.H.; Samuel, A.M.; Doty, H.W.; Valtierra, S.; Samuel, F.H. Effect of additives on the microstructure and tensile properties of Al-Si alloys. *J. Mater. Res. Technol.* **2019**, *8*, 2255–2268. [[CrossRef](#)]
6. Sjölander, E.; Seifeddine, S. The heat treatment of Al-Si-Cu-Mg casting alloys. *J. Mater. Process. Technol.* **2010**, *210*, 1249–1259. [[CrossRef](#)]
7. Salleh, M.S.; Hanizam, O.; Mohd, Z.S.; Abu, B.A.R.; Soufhwee, Y.; Saifudin, H.A.R.; Mohd, W.A.Z. T6 heat treatment optimization of thixoformed LM4 aluminium alloy using response surface methodology. *Malays. J. Compos. Sci. Manuf.* **2020**, *3*, 1–13. [[CrossRef](#)]

8. Mukund, A.; Aditya, S.N.; Raagavendran, S.; Premkumar, R.; Akhil, R.; Nidhin Shankar, A.; Karthik, V. Impact of solutionising temperature on the microstructure, hardness and tensile strength of Al-6.6Si-0.3Mg-3Ni alloys. *Mater. Today Proc.* **2021**, *38*, 2117–2122. [[CrossRef](#)]
9. Yang, H.; Ji, S.; Yang, W.; Wang, Y.; Fan, Z. Effect of Mg level on the microstructure and mechanical properties of die-cast Al-Si-Cu alloys. *Mater. Sci. Eng. A* **2015**, *642*, 340–350. [[CrossRef](#)]
10. Srinivas, D.; Sharma, S.; Gowrishankar, M.C.; Hiremath, P.; Shettar, M. Effect of single and multistage solution heat treatment on age hardened A319 alloy. *AIP Conf. Proc.* **2022**, *2421*, 040001. [[CrossRef](#)]
11. Samuel, A.M.; Doty, H.W.; Valtierra, S.; Samuel, F.H. Relationship between tensile and impact properties in Al-Si-Cu-Mg cast alloys and their fracture mechanisms. *Mater. Des.* **2014**, *53*, 938–946. [[CrossRef](#)]
12. Li, Z.; Limodin, N.; Tandjaoui, A.; Quaegebeur, P.; Witz, J.F.; Balloy, D. Damage investigation in A319 aluminum alloy by digital image correlation during in-situ tensile tests. *Procedia Struct. Integr.* **2016**, *2*, 3415–3422. [[CrossRef](#)]
13. Li, Z.; Limodin, N.; Tandjaoui, A.; Quaegebeur, P.; Witz, J.F.; Balloy, D. In-situ 3D characterization of tensile damage mechanisms in A319 aluminium alloy using X-ray tomography and digital volume correlation. *Mater. Sci. Eng. A* **2020**, *794*, 139920. [[CrossRef](#)]
14. Samuel, E.; Golbahar, B.; Samuel, A.M.; Doty, H.W.; Valtierra, S.; Samuel, F.H. Effect of grain refiner on the tensile and impact properties of Al-Si-Mg cast alloys. *Mater. Des.* **2014**, *56*, 468–479. [[CrossRef](#)]
15. Han, Y.; Samuel, A.M.; Doty, H.W.; Valtierra, S.; Samuel, F.H. Optimizing the tensile properties of Al-Si-Cu-Mg 319-type alloys: Role of solution heat treatment. *Mater. Des.* **2014**, *58*, 426–438. [[CrossRef](#)]
16. Rincon, E.; Lopez, H.F.; Cisneros, M.M.; Mancha, H. Temperature effects on the tensile properties of cast and heat treated aluminum alloy A319. *Mater. Sci. Eng. A* **2009**, *519*, 128–140. [[CrossRef](#)]
17. Zhu, M.; Jian, Z.; Yang, G.; Zhou, Y. Effects of T6 heat treatment on the microstructure, tensile properties, and fracture behavior of the modified A356 alloys. *Mater. Des.* **2012**, *36*, 243–249. [[CrossRef](#)]
18. Poria, S.; Sahoo, P.; Sutradhar, G. Design of experiments analysis of wear behavior of stir cast Al-TiB<sub>2</sub> composite in lubricated condition. *Mater. Today Proc.* **2018**, *5*, 5221–5228. [[CrossRef](#)]
19. Karbalaei Akbari, M.; Baharvandi, H.R.; Shirvanimoghaddam, K. Tensile and fracture behavior of nano/micro TiB<sub>2</sub> particle reinforced casting A356 aluminum alloy composites. *Mater. Des.* **2015**, *66*, 150–161. [[CrossRef](#)]
20. Xiao, C.; Hong-Tao, W.; Gang-Chang, J.; Xiao-Bo, B.; Wei, F. Microstructure and properties of TiB<sub>2</sub>-Ni coatings with different binder phase contents deposited by HVOF spray process. *Rare Met.* **2022**, *41*, 1385–1393. [[CrossRef](#)]
21. Vandersluis, E.; Ravindran, C. Effects of solution heat treatment time on the as-quenched microstructure, hardness and electrical conductivity of B319 aluminum alloy. *J. Alloys Compd.* **2020**, *838*, 155577. [[CrossRef](#)]
22. Akhil, M.G.; Preenu, S.; Hari, S.; Ravi, M. Effect of heat treatment on the mechanical properties of squeeze-cast Al-5Si-3Cu alloy for automotive applications. *Trans. Indian Inst. Met.* **2019**, *72*, 1129–1132. [[CrossRef](#)]
23. Sokolowski, J.H.; Djurdjevic, M.B.; Kierkus, C.A.; Northwood, D.O. Improvement of 319 aluminum alloy casting durability by high temperature solution treatment. *J. Mater. Process. Technol.* **2001**, *109*, 174–180. [[CrossRef](#)]
24. Mohamed, A.M.A.; Samuel, F.H.; Al kahtani, S. Influence of Mg and solution heat treatment on the occurrence of incipient melting in Al-Si-Cu-Mg cast alloys. *Mater. Sci. Eng. A* **2012**, *543*, 22–34. [[CrossRef](#)]
25. Srinivas, D.; Shankar, G.; Sharma, S.; Shettar, M.; Hiremath, P. Artificial neural network for predicting hardness of multistage solutionized and artificially aged LM4 + TiB<sub>2</sub> composites. *Mater. Res.* **2022**, *25*, 2022. [[CrossRef](#)]
26. MC, G.; Hiremath, P.; Shettar, M.; Sharma, S.; Rao, U.S. Experimental validity on the casting characteristics of stir cast aluminium composites. *J. Mater. Res. Technol.* **2020**, *9*, 3340–3347. [[CrossRef](#)]
27. Shettar, M.; Hiremath, P.; Shankar, G.; Kini, A.; Sharma, S. Tribolayer behaviour and wear of artificially aged Al6061 hybrid composites. *Int. J. Automot. Mech. Eng.* **2021**, *18*, 8668–8676. [[CrossRef](#)]
28. Jayashree, P.K.; Gowrishankar, M.C.; Sharma, S.; Shetty, R.; Shettar, M.; Hiremath, P. Influence of homogenization and aging on tensile strength and fracture behavior of TIG welded Al6061-SiC composites. *J. Mater. Res. Technol.* **2020**, *9*, 3598–3613. [[CrossRef](#)]
29. Donald, R.; Askeland, D.K.B.; Pradeep, P.F. *Essentials of Materials Science and Engineering*, 4th ed.; Cengage Learning, Inc.: Boston, MA, USA, 2010.
30. Medrano-Prieto, H.M.; Garay-Reyes, C.G.; Gómez-Esparza, C.D.; Aguilar-Santillán, J.; Maldonado-Orozco, M.C.; Martínez-Sánchez, R. Evolution of microstructure in Al-Si-Cu system modified with a transition element addition and its effect on hardness. *Mater. Res.* **2016**, *19*, 59–66. [[CrossRef](#)]
31. Hwang, J.Y.; Banerjee, R.; Doty, H.W.; Kaufman, M.J. The effect of Mg on the structure and properties of Type 319 aluminum casting alloys. *Acta Mater.* **2009**, *57*, 1308–1317. [[CrossRef](#)]
32. Milan, M.T.; Bowen, P. Tensile and fracture toughness properties of SiC<sub>p</sub> reinforced Al alloys: Effects of particle size, particle volume fraction, and matrix strength. *J. Mater. Eng. Perform.* **2004**, *13*, 775–783. [[CrossRef](#)]
33. Carlo, A.B.; Paola, B.; Jacopo, F.; Mihaela, A.; Ausonio, T. Selective laser melting of AlCu-TiB<sub>2</sub> alloy using pulsed wave laser emission mode: Processability, microstructure and mechanical properties. *Mater. Des.* **2021**, *204*, 109628. [[CrossRef](#)]
34. Siddique, R.A.; Abdul-Wahab, S.A.; Pervez, T. Effect of aging time and aging temperature on fatigue and fracture behavior of 6063 aluminum alloy under seawater influence. *Mater. Des.* **2008**, *29*, 70–79. [[CrossRef](#)]
35. Herbert, M.A.; Das, G.; Maiti, R.; Chakraborty, M.; Mitra, R. Tensile properties of cast and mushy state rolled Al-4.5Cu alloy and in situ Al4.5Cu-5TiB<sub>2</sub> composite. *Int. J. Cast Met. Res.* **2015**, *23*, 216–224. [[CrossRef](#)]